JACS
JOURNAL OF THE AMERICAN CHEMICAL SOCIETY
Article
pubs.acs.org/JACS

Nanoscale Plasma Chemistry Enables Fast, Size-Selective Nanotube Nucleation

Kostya (Ken) Ostrikov*[,‡,†] and Hamid Mehdipour[‡,§,†]

[‡]Plasma Nanoscience Centre Australia (PNCA), CSIRO Materials Science and Engineering, P.O. Box 218, Lindfield, New South Wales 2070, Australia, and Plasma Nanoscience @ Complex Systems, School of Physics, The University of Sydney, New South Wales 2006, Australia

[§]Department of Physics, Faculty of Basic Science, University of Mazandaran, P. O. Box 47416-1467, Babolsar, Iran

Supporting Information

ABSTRACT: The possibility of fast, narrow-size/chirality nucleation of thin single-walled carbon nanotubes (SWCNTs) at low, device-tolerant process temperatures in a plasma-enhanced chemical vapor deposition (CVD) is demonstrated using multiphase, multiscale numerical experiments. These effects are due to the unique nanoscale reactive plasma chemistry (NRPC) on the surfaces and within Au catalyst nanoparticles. The computed three-dimensional process parameter maps link the nanotube incubation times and the relative differences between the incubation times of SWCNTs of different sizes/chiralities to the main plasma- and precursor gas-specific parameters and explain recent experimental observations. It is shown that the unique NRPC leads not only to much faster nucleation of thin nanotubes at much lower process temperatures, but also to better selectivity between the incubation times of SWCNTs with different sizes and chiralities, compared to thermal CVD. These results are used to propose a time-programmed kinetic approach based on fast-responding plasmas which control the size-selective, narrow-chirality nucleation and growth of thin SWCNTs. This approach is generic and can be used for other nanostructure and materials systems.

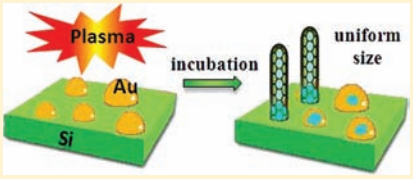

1. INTRODUCTION

Chirality-selective synthesis of single-walled carbon nanotubes (SWCNTs) at low, nanodevice-tolerable temperatures, while minimizing precursor atom consumption, still remains a major science challenge on the way of their widespread applications in nanoelectronics, information processing and storage, renewable energy, environmental, biomedical, and other technologies.[1−5] Despite almost two decades of research, the underlying mechanisms of this still elusive ability still remain essentially unclear, mostly because of the very large number of the process- and catalyst-specific parameters and effects involved. These effects are related to the process temperature, delivery and loss of precursor species, formation of the initial nuclei and SWCNT caps, as well as defect incorporation during the nucleation or growth stages; these phenomena are commonly studied quite separately.[6−11] This is the reason unifying strategies to resolve this challenge based on the understanding of the nanotube nucleation and growth kinetics in its entirety are highly warranted.

Catalyst nanoparticle (CNP) supersaturation with carbon, graphene monolayer (GML) formation, and bending, followed by the stable cap formation and lifting off from the CNP surface is commonly recognized as the most important chirality-determining stage.[12,13] The completion of this stage is heralded by the onset of the diameter-selective photoluminescence emission (PLE) and is quantified by the incubation time t_i.[14−16] This time is different for nanotubes of different sizes and chiralities. Therefore, by precisely controlling the supply of carbon atoms and energy to catalyst nanoparticles of different sizes, it is plausible to achieve time-resolved nucleation of the nanotubes of only the desired thickness and chirality.[17,18]

However, this is extremely difficult to achieve in practice for several reasons. First, reliable experimental data on the SWCNT incubation times is very limited because of its process- and nanotube-specific nature and measurement complexity.[2,13,15] This is the reason predictive numerical modeling to elucidate the effects of the catalyst and process parameters on t_i of the nanotubes of different sizes is indispensable and is carried out in this work. Second, selective growth of SWCNTs with narrow size/chirality distributions poses several significant challenges.[15,19] Indeed, as the growth continues beyond the incubation time of the nanotubes of the desired size/chirality range, SWCNTs of many other sizes/chiralities may also nucleate and grow after their respective incubation times elapse. This is the reason the incubation times should be as short as possible and the relative differences between the incubation times of the nanotubes of different sizes/chiralities should be as large as possible. In this case, it may be possible to quickly adjust the process conditions to continue the growth of the as-nucleated SWCNTs of the desired sizes/chiralities while disabling the nucleation of other nanotubes.

The incubation times can be reduced by increasing the substrate temperatures and/or precursor gas pressures.[15] However, given the already very high temperatures required

Received: November 17, 2011
Published: February 2, 2012

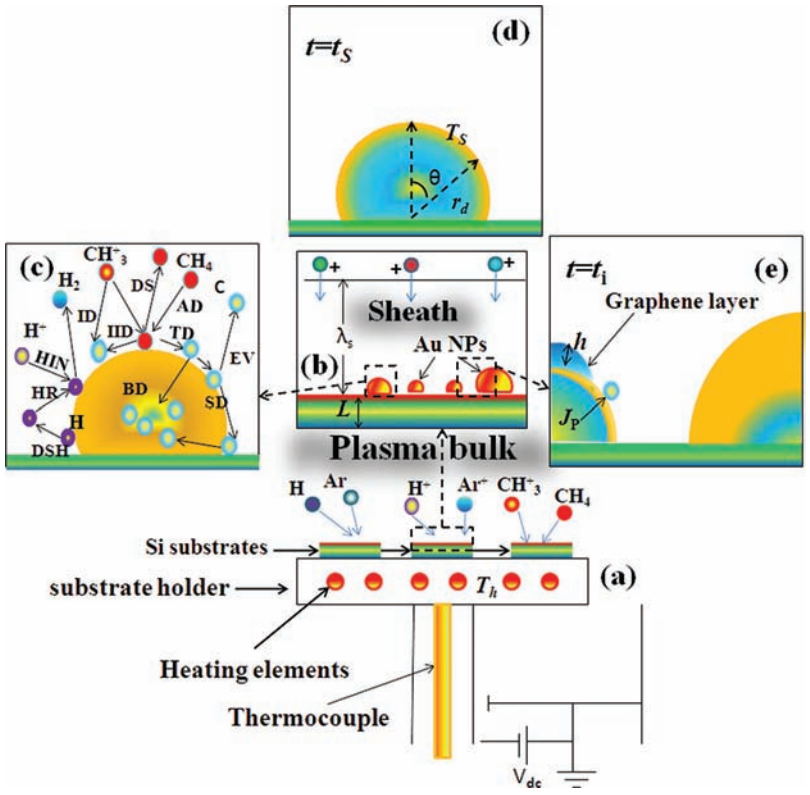

Figure 1. Schematic of the effect of the nanoscale reactive plasma chemistry on nucleation and bending of a graphene monolayer on a Au catalyst nanoparticle. Species deposition (a), sheath geometry (b), hydrogen plasma species-induced processes on the Au CNP surface (c), CNP saturation with carbon (d), and carbon atom extrusion (denoted by J_P in panel (e)), GML nucleation and then bending (e) in reactive $Ar/H_2/CH_4$ plasmas. The elementary processes associated with the nanoscale reactive plasma chemistry (NRPC) (c) are ion-induced dissociation (IID), ion decomposition (ID), hydrogen recombination (HR), hydrogen ion-induced neutralization (HIN), adsorption of hydrogen atoms (ADH), desorption of hydrogen atoms (DSH), adsorption (AD) and desorption (DS) of CH_3 radicals, evaporation (EV) and surface diffusion (SD) of C atoms and thermal dissociation of CH_3 (TD).

for thin SWCNT nucleation, any further temperature increase is undesirable not only from the nanodevice tolerance requirements, but also because of the much better size/chirality selectivity of the nanotube nucleation at lower temperatures.[15,20,21] Increasing precursor gas pressures is also undesirable because of the apparent risks of catalyst overfeeding, which may lead to the formation of other carbon structures (e.g., multiwalled CNTs, nanofibers, nanowires, or nanocages), or even complete CNP burying even before the nanotube incubation is complete. Thus, delivery of carbon atoms should be precisely dosed and, ideally, also localized on or near the surface of catalyst nanoparticles. On the other hand, the ability to quickly adjust the process parameters (e.g., precursor species delivery and catalyst heating) requires a flexible, fast-responding process environment. Unfortunately, in most common thermal chemical vapor deposition (CVD) systems, it appears very difficult to quickly adjust heat supply and precursor gas flows.[22]

These issues may be mitigated in low-temperature plasmas, which feature dry reactive gas-phase chemistry, very fast responses of the ionized component (electrons, ions, and charged radicals) to electromagnetic fields, effective control of building unit (BU) production both in the gas phase and on the surface, localized heating of merely the topmost atomic layers on the surface, and many other unique properties not common to neutral gas and wet chemistries.[13,16,23−28] Recent experiments have demonstrated the possibility to achieve narrow size/chirality distributions of thin SWCNTs on small CNPs, in the plasma at low process temperatures.[15,17−20,29−31] Moreover, by generating the plasma for a relatively short, limited time during the CVD process, it is possible not only to improve the size/chirality selectivity, but to also produce very short SWCNTs with fairly uniform length distribution.[17] However, the size/chirality-selective, time-programmed SWCNT growth still remains elusive, mainly because of the lack of reliable information on the link between the nanotube thickness, incubation times, catalyst material/size, and the process parameters.[15]

This work contributes to establishing the above missing links by using multiscale, multiphase numerical modeling of SWCNT nucleation in low-temperature plasmas. It is shown that nanoscale reactive plasma chemistry localized across the surface of Au catalyst nanoparticles enables faster, lower-temperature nucleation of SWCNTs compared to the equivalent thermal CVD. This study also confirms competitive advantages of the plasma-enhanced CVD (PECVD) in the size selectivity of SWCNT nucleation at low temperatures, on small catalyst nanoparticles and provides three-dimensional process parameter maps that link the incubation times of SWCNTs of different sizes/chiralities to the main process parameters. The parameter spaces where relative differences between the incubation times of the nanotubes of different sizes/chiralities (and hence, the selectivity of nucleation) can be increased compared to thermal CVD are identified as well. On the basis of these results, we also propose a viable approach toward fast, time-programmed, size-selective nucleation and growth of thin single-walled carbon

dx.doi.org/10.1021/ja210813s | J. Am. Chem. Soc. 2012, 134, 4303−4312

nanotubes with narrow chirality distributions, at low process temperatures. This approach is generic and can be used for a broader range of thermal gas/vapor-phase reactive chemistries and nanostructure growth processes.

2. RESULTS AND DISCUSSION

2.1. Nanoscale Plasma Chemistry and SWCNT Nucleation. Figure 1 shows a schematic of the SWCNT nucleation on Au catalyst nanoparticles on a Si substrate exposed to the reactive plasma in a $Ar/H_2/CH_4$ gas mixture commonly used for carbon nanostructure synthesis.[2] The substrate is supported by a substrate holder externally heated to temperature T_h (Figure 1a). Our multiscale, multiphase model covers the main stages of the SWCNT nucleation which includes BU production and transport to CNPs, energy and matter exchange on the CNP surface, carbon surface and bulk diffusion, catalyst nanoparticle saturation, followed by the nucleation and bending of a graphene monolayer on the Au surface. The model comprises the plasma sheath, ion/radical transport (Figure 1b), species creation/loss, plasma−surface interactions, heat transfer, surface/bulk diffusion (Figure 1c), as well as CNP saturation (Figure 1d), GML nucleation and bending/liftoff numerical modules (Figure 1e). The model and the main processes/reactions involved are briefly described in the Models and Computational Methodology section, with more details provided in the Supporting Information.

The main focus in this work is on the nanoscale plasma-surface chemistry (NPSC) sketched in Figure 1a−c. For the sake of transparency and clarity, let us outline and briefly explain what one could expect to achieve (and was achieved in the numerical experiments of this work, see sections 2.2−2.5) by capitalizing on the NRPC effects. The localized, nanoscale plasma-surface interactions produce carbon atoms directly on the CNP surface through a number of reactions,[21,32] including ion-assisted reactions unique to the ionized gas environments (Figure 1c). These interactions also provide significant heat, additional to the external substrate heating. As a result, the number of carbon atoms available for the GML nucleation and the CNP temperature can be increased. This leads to the faster catalyst supersaturation with carbon (Figure 1d).

Plasma-enhanced surface diffusion supplemented by the stronger outward flux of the carbon atoms enhanced by the Gibbs−Thomson (GT) effect[21,35] also leads to the faster nucleation of the graphene monolayer on the top surface of the CNP (Figure 1d,e). The GT effect is quantified by the difference in chemical potentials within and on the surface of the catalyst nanoparticle $\Delta\mu^{GT}$ and is stronger for smaller CNPs. Moreover, $\Delta\mu^{GT}$ in the plasma case is larger than in thermal CVD; hence, the GT effect is stronger in the plasma, for smaller nanoparticles.

Hence, the GT and plasma effects play constructively to increase the kinetic energy of carbon atoms E_K thereby increasing the GML bending energy $\Delta E = E_K - W_{ad}$, where W_{ad} is the work of adhesion (per unit area) of the GML to the catalyst surface. This is the reason nucleation of thin SWCNTs may happen particularly faster on small CNPs exposed to the plasma. Therefore, one can expect the incubation times t_i of thin SWCNTs in the PECVD to be significantly shorter than in thermal CVD.

More importantly, the plasma conditions can be quickly modified right afterward to alter the heating and BU supply on the CNPs thereby disabling the nucleation of thicker nanotubes eventually leading to size-selective growth of SWCNTs with narrow chirality distributions. These features and qualitative predictions, complemented with the improved selectivity of incubation times in the plasma-assisted SWCNT growth, are quantified and discussed below.

2.2. Plasma Effects: Faster Nucleation, Thinner Nanotubes. Figure 2 shows the dependencies of the critical diameter

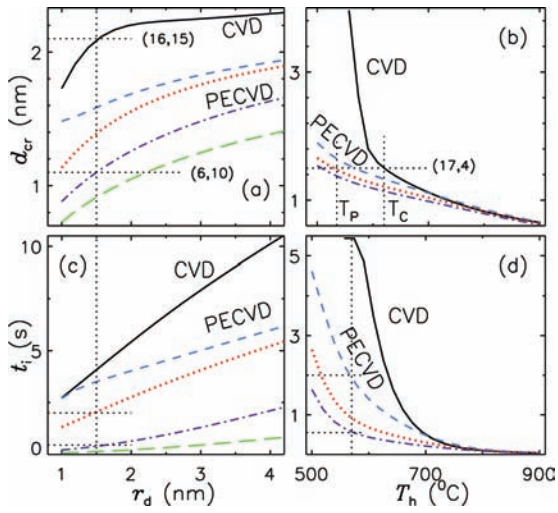

Figure 2. The critical diameter for GML nucleation d_{cr} (a and b) and incubation time t_i (c and d) as functions of the CNP radius r_d and substrate holder temperature T_h for CVD (solid curve) and PECVD (dashed, dotted, dash-dotted, and long dashed curves) for electron temperature T_e = 1.0 eV, ion temperature T_i = 0.05 eV, total gas pressure p_0 = 50 mTorr, surface potential Φ_S = −100 V, and percentage of hydrogen in the gas mixture r_H = 10%. The dashed, dotted, dash-dotted, and long dashed curves in panels a and c correspond to the plasma density $n_{e0} = 5 \times 10^{10}$, 5×10^{11}, 5×10^{12}, and 1.5×10^{13} cm^{-3}, respectively, while the dashed, dotted, and dash-dotted curves in panels b and d correspond to T_e = 1.0, 2.5, and 4.0 eV, respectively. In panels a and c, percentage of Ar r_{Ar} = 85%, percentage of methane r_{CH} = 5%, substrate holder temperature T_h = 580 °C. In panels b and d, $n_{e0} = 5 \times 10^{11}$ cm^{-3}, r_{Ar} = 80%, r_{CH} = 10%, and r_d = 2 nm. Nucleation of thin (6,10) and thick (16,15) semiconducting nanotubes is shown as a representative example. Also, T_C and T_P are the temperatures for the nucleation of a (17,4) semiconducting nanotube in CVD and PECVD, respectively.

d_{cr} (the minimum possible nanotube thickness) and the incubation time t_i on the CNP radius r_d [panels a and c] and the substrate holder temperature T_h [panels b and d] in CVD and PECVD at the same precursor gas and external heating conditions. One can clearly see that much thinner SWCNTs can nucleate in PECVD on catalyst particles of the same radius and other CVD conditions. In the example shown in Figure 2a, a (6,10) nanotube with the diameter of ∼1.1 nm can nucleate on a CNP with the radius r_d = 1.5 nm in a plasma, while a much thicker (16,15) SWCNT of a diameter of ∼2.1 nm is expected to nucleate in thermal CVD. The nucleation temperatures can also be substantially reduced in the plasma-based process. As Figure 2b suggests, the temperature difference $T_P - T_C$ for the nucleation of a (17,4) semiconducting nanotube in PECVD (T_P) and CVD (T_C) is approximately 85 K. In this case, T_P is even ∼25 K lower than the lowest temperature when any SWCNT nucleation is possible in the equivalent neutral gas-based process. The results in Figure 2a,b show a consistent trend of a gradual reduction of the critical diameter and the external heating temperature with the increase of the plasma

dx.doi.org/10.1021/ja210813s | J. Am. Chem. Soc. 2012, 134, 4303−4312

density and the electron temperature, and hence, the number of the plasma ions interacting with the surface of the Au nanoparticle.

Plasma generation in the otherwise neutral $Ar/H_2/CH_4$ gas mixture significantly shortens the incubation time, which also decreases as the catalyst nanoparticles get smaller. From Figure 2c, one finds that for a CNP with a radius of 1.5 nm, the incubation time may be reduced from almost 4 s in CVD to less than 0.5 s in PECVD. The nanotubes can nucleate much faster at the same temperature of external heating. Indeed, from Figure 2c one can see that more than 5 s is needed to nucleate a GML on a Au nanoparticle with a radius of 2 nm. By generating the plasma and then increasing its density n_{e0} from 5×10^{11} to 5×10^{12} cm^{-3}, it is possible to reduce t_i to ~2.0 s and then further to only ~0.45 s. A similar effect can be achieved by increasing the electron temperature as can be seen from Figure 2d. Indeed, by increasing the electron temperature T_e from 1.0 to 4.0 eV, it is possible to reduce t_i to 1.95 and then further to only ~0.55 s. The incubation time becomes shorter in the plasma environment since the incubation time is inversely proportional to the flux of carbon atoms into the catalyst nanoparticle while the carbon flux into the catalyst increases when the plasma is generated. This happens because the plasma ions, impinging on the catalyst surface, collide with hydrocarbon radicals or undergo decomposition (due to collisions with the surface). As a result, more carbon atoms are produced and diffuse into the catalyst. Because of the stronger fluxes of carbon atoms extruded through the catalyst, the AuC alloy is saturated quickly which is followed by faster C precipitation (as a result of a larger chemical potential in the alloy).

The decreasing trend of the incubation time with the "strength" of the plasma (characterized in this example by the higher plasma densities or other plasma-related parameters such as the electron temperature and the surface potential) is consistent: the larger the parameters specifically related to the plasma are, the shorter the incubation time is. This can be understood by noting that when the plasma density increases so does the ion flux to the CNP surface. This enhanced ion-surface interaction simultaneously leads not only to more effective surface heating, but also to the larger number of carbon atoms produced through the ion-assisted reactions sketched in Figure 1c. This trend is consistent with the experimental results of Ghorannevis et al., where much shorter incubation times were reported for the plasma-assisted SWCNT nucleation compared with the thermal CVD one.[20] Moreover, the results in Figure 2 also confirm the experimental trend of a significant increase of the nanotube incubation times when the input power (and hence the amount of carbon material supply) is decreased.[17]

More importantly, the numerical values of t_i computed in our study are reasonably close to the incubation times deduced experimentally from the PLE imaging.[14,17−20] The experimental values appear to be higher compared to our calculations. This is very reasonable because of the minimum extent of the SWCNT cap detachment and possible elongation with respect to the catalyst nanoparticle surface required for the PLE signal detection, which our models do not take into account. Moreover, the shortest experimental runs are usually chosen longer than the values of t_i computed in this work. This leaves the possibility of even earlier detection of SWCNT nucleation plausible; this possibility would substantially improve the quantitative agreement with the experimental results.

The results in Figure 2 also suggest that in PECVD, as the CNP radius decreases, the sizes of graphene nuclei also decrease in a stronger-than-linear fashion. In this case, the incubation times decrease while the bending energies become much higher; these trends are also nonlinear, particularly for small CNPs with r_d < 1.5 nm (see Figure S1a in Supporting Information). Therefore, smaller *stable* (capable of detaching and lifting from the catalyst surface) SWCNT caps feature shorter incubation times compared to the larger caps. This means that thinner SWCNTs indeed nucleate faster. Therefore, using time-controlled plasma exposure, one can synthesize SWCNTs with significantly narrower diameter and, hence, also the chirality distributions. This is in a good agreement with the appearance of very thin SWCNTs with narrow chirality distributions at early stages (typically 2−10 s, which is consistent with our numerical results) in the recent experiments.[17,20,30]

2.3. Improved Selectivity of Incubation Times. To illustrate the effect of the plasma on the selectivity of the incubation times, we have calculated the absolute values of the relative differences τ_{sel} in t_i of a number of selected nanotubes with respect to the incubation times of the nanotubes of the average size t_{av}. The strength of the plasma parameters (e.g., the plasma density in Table 1) was varied and the results compared with the equivalent CVD case. Table 1 presents these results for 4 semiconducting and 2 metallic nanotubes (according to the natural 2:1 expectancy ratio) in a thermal CVD and in a PECVD with the increased values of the plasma density n_{e0} (which is the same as the ion density n_i due to the overall charge neutrality of the plasma).

Table 1. The Selectivity of the Nanotube Incubation Times τ_{sel} (= $|(t_i - t_{av})/t_{av}|$) Computed for the Metallic (Boldfaced) and Semiconducting SWCNTs with Different Diameters in Thermal CVD (n_{e0} = 0), and Three PECVD (n_{e0} = 5×10^{12}, 1.5×10^{13}, and 5×10^{13} cm^{-3}) Cases[a]

	$\tau_{sel} = \lvert(t_i - t_{av})/t_{av}\rvert$			
d_{cr}[nm] (m,n)	n_{eo} = 0 (CVD)	n_{eo} = 5×10^{12} cm^{-3}	n_{eo} = 1.5×10^{13} cm^{-3}	n_{eo} = 3×10^{13} cm^{-3}
0.93 (0,12)	0.770	0.936	0.942	0.910
1.43 (8,13)	0.472	0.709	0.743	0.662
1.73 (4,20)	0.146	0.237	0.273	0.208
1.90 (1,24)	0.148	0.266	0.285	0.238
2.01 (9,20)	0.431	0.745	0.846	0.648
2.08 (9,21)	0.707	1.198	1.384	1.028

[a]The incubation times of the SWCNTs with the average size (with diameters 2.3 nm for the CVD, and 1.8, 1.5, and 1.29 nm for the 3 PECVD cases, respectively) have been chosen as t_{av}.

These results suggest that the selectivity of the incubation times appears to be better in the plasma-based process. In Table 1, this improvement ranges from ~50% to almost two times. More importantly, τ_{sel} increases consistently with the plasma density, from very low values up to a certain threshold, which is ~2.0×10^{13} cm^{-3} in the case considered. Therefore, by excessively increasing the plasma density (e.g., increasing the input power), the nanotube size selectivity can be diminished quite significantly (by a couple of tens percent in the examples shown in Table 1). However, the computed threshold for the continued increase of the SWCNT nucleation selectivity (n_{e0} ~ 2.0×10^{13} cm^{-3}) is well above typical plasma densities

dx.doi.org/10.1021/ja210813s | J. Am. Chem. Soc. 2012, 134, 4303−4312

achievable in low-pressure plasma-assisted synthesis of single-walled carbon nanotubes.[15] Hence, the computed trend of the improved selectivity of the nanotube incubation times with the higher plasma density appears to be consistent.

More importantly, as the plasma/ion density increases, localized carbon production via the NRPC reactions (see Figure 1) becomes more effective. In other words, carbon material supply increases, which was experimentally achieved by raising the input power P_{in};[17] higher P_{in} usually produces higher plasma/ion densities. A striking observation was made that under such conditions not only the incubation times dramatically decreased, but also the nanotube chirality selectivity much improved.[17] The results of our numerical experiments clearly confirm these experimental results. Therefore, the plasma exposure does improve the selectivity of the SWCNT incubation times and this selectivity also improves as the plasma density increases.

2.4. 3D Parameter Maps: Plasma Effects. The plasma density is one of the easiest-to-control plasma parameters which can respond very quickly to the variation of the process parameters such as P_{in}. However, other process parameters may also play a major role in enabling effective control of the nanotube incubation times. Therefore, we have computed three-dimensional parameter maps that link t_i with the process parameters and the expected critical diameter of the nanotube to nucleate. In this subsection, we show the effects of the plasma-specific parameters, such as the plasma density n_{e0}, electron temperature T_e, and the surface potential Φ_S. The surface potential can be easily controlled by varying the electric bias applied to the surface. Pulsed DC bias is particularly promising for time-programmed SWCNT growth. The electron temperature is also an essential characteristic of the plasma; it can also be controlled by the process conditions.

The 3D graded color plots in Figure 3 relate the incubation time to the GML critical diameter and n_{e0} (a), T_e (b), and Φ_S (c). In Figures 3 and 4, two semiconductor (of (6,5) and (8,4) chiralities) and one (15,0) zigzag metallic SWCNTs are marked to identify the appropriate conditions for their nucleation. It is clearly seen that the incubation times become shorter for smaller critical diameters (thus, smaller (6,5) and (8,4) SWCNTs considered here) and higher values of the plasma density, electron temperature, and the magnitude of the surface potential. This trend is explained by noting that all the changes (in T_e, n_{e0}, and Φ_S to higher values) lead to stronger fluxes of the plasma ions onto the CNP surface. This gives rise to more effective heating of the CNP surface (through the ion-surface interactions) and also effective carbon atom production through ion-induced dissociation of precursor species on the catalyst surface. As a result, the catalyst becomes hotter, and the number of carbon atoms on its surface increases. This leads to faster nucleation of smaller GMLs on smaller CNPs. Under such conditions, the bending energy also increases which eventually results in the rapid nucleation of thin SWCNTs with a narrow size distribution.

The results in Figure 3 also suggest that the relative selectivity of incubation times can be improved by increasing the plasma-specific parameters. For example, the relative difference in the incubation times between the thin (8,4) and thicker (15,0) nanotubes which is ~0.48 s at $n_{e0} \sim 2 \times 10^{11}$ cm^{-3} increases to almost 0.75 s at $n_{e0} \sim 3 \times 10^{12}$ cm^{-3} (Figure 3a). A somewhat similar effect can be deduced from Figure 3c, where the influence of the surface potential is quantified. The effect of the electron temperature, while very significant on the

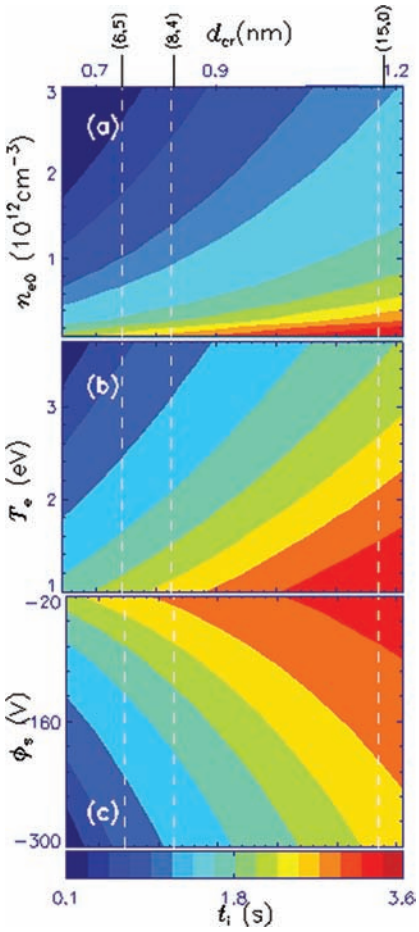

Figure 3. The link in a three-dimensional parameter space between the plasma-related parameters [(a) plasma density n_{e0}; (b) electron temperature T_e; and (c) surface potential Φ_S], the critical diameter d_{cr}, and the incubation time in the plasma-based SWCNT growth process. Unless varied in any particular plot, the default set of parameters is T_e = 1.0 eV, T_i = 0.05 eV, $n_{e0} = 10^{11}$ cm^{-3}, P_0 = 50 mTorr, Φ_S = −100 V, r_{Ar} = 70%, r_{CH} = 20%, r_H = 10%, and T_H = 600 °C. Examples of (6,5) and (8,4) semiconducting and (15,0) metallic nanotubes are shown.

incubation time, is less pronounced for the selectivity of t_i. An increase of T_e from 1.0 to 3.0 eV leads to a very small change (~0.1 s) of the difference between the incubation times of the two selected nanotubes (Figure 3b). Nevertheless, since the incubation time for the both nanotubes decreased quite significantly, the relative selectivity of the nucleation onsets can be significantly improved by using plasmas with a higher electron temperature.

The results presented in 3D parameter maps in Figure 3 further confirm the experimental observations suggesting that the SWCNT incubation times are very sensitive to the carbon material supply.[15,17,18,20] In the following subsection, we will consider the effects of the precursor gas pressure and composition.

2.5. 3D Parameter Maps: Effects of Precursor Gas. Three-dimensional graded color plots in Figure 4 show the links between the SWCNT nucleation time, GML critical diameter, and the working gas pressure P_0 (Figure 4a) and composition of the gas mixture (Figure 4b). The latter is represented by the percentage of hydrogen r_H, which is an indicator of the chemical reactivity of the gas mixture. It is clearly seen that the incubation time decreases with decreasing

dx.doi.org/10.1021/ja210813s | J. Am. Chem. Soc. 2012, 134, 4303−4312

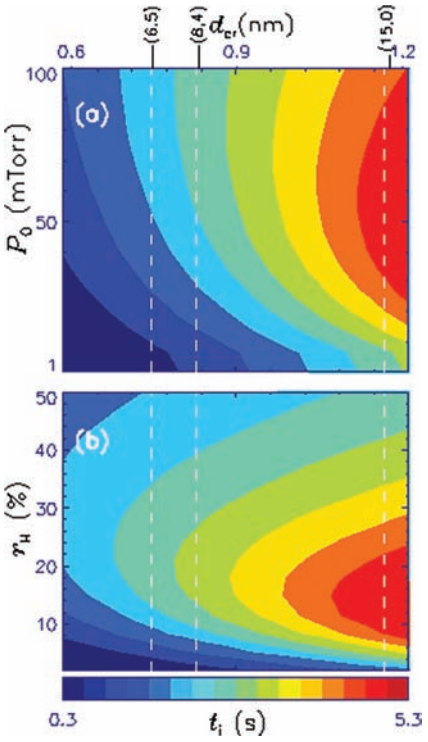

Figure 4. The link in a three-dimensional parameter space between the parameters of the precursor gas mixture [(a) total pressure P_0; (b) percentage of hydrogen gas r_H], the critical diameter d_{cr}, and the incubation time in the plasma-based SWCNT growth process. The default set of parameters and the nanotube examples are the same as in Figure 3.

the total gas pressure; this dependence becomes even stronger for smaller critical diameters. The bending energy is also higher at lower P_0 (see Figure S2c in the Supporting Information). This explains the experimental observations that thin SWCNTs with a narrow diameter distribution nucleate better at lower gas pressures.[30,31] This happens because the plasma sheath becomes wider at lower total gas pressures. By traversing this wider sheath, the ions are able to gain larger amounts of energy. As a result, the ion-induced heating and carbon production reactions (on the nanoscale catalyst surface) become more effective. Thus, the C concentration on the CNP surface increases, which leads to the formation of small graphene nuclei.

A striking observation from Figure 4a is that the incubation times are shorter at lower total gas pressures. This observation is rather unexpected because of the expected larger supply of hydrocarbon precursor species (and hence, faster CNP supersaturation) at higher total gas pressures. This effect is to a very large extent due to the nanoscale reactive plasma chemistry, which leads to much faster production of carbon atoms on the CNP surface via localized ion-assisted reactions (sketched in Figure 1) at lower total gas pressures. This result is also in accord with the conclusion that the increased supply of hydrocarbon precursor is probably not the key factor in the improved SWCNT size/chirality distribution observed in the recent experiments.[17] Indeed, delivery of larger amounts of hydrocarbons to the whole surface is not as important as the production of carbon atoms where they are actually needed on the CNP surface, by using the NRPC effects.

The variation of the SWCNT incubation times with the percentage of hydrogen in the $Ar/CH_4/H_2$ gas mixture in Figure 4b is very nonlinear and shows the opposite trends at lower and higher r_H . For each of the 3 nanotubes highlighted in this example, the incubation time first increases and then decreases again as the hydrogen percentage gets higher. The first increase in t_i with increasing r_H can be attributed to the more effective interaction of carbon atoms with hydrogen atoms due to stronger hydrogen atom/ion fluxes to the CNP surface. With a further increase of r_H, the catalyst heating induced by the HR and HIN processes (Figure 1c) prevails over the C atom loss. In this case, the catalyst surface becomes hotter, which results in a more effective thermal dissociation of hydrocarbon precursor species. As a result, the concentration of carbon atoms in the AuC alloy increases, which tends to reduce the incubation time. The two counteracting effects lead to the gradual reversal of the incubation time trend with the additional supply of hydrogen gas. The same trend can be observed for the GML critical diameter and an interesting reverse trend is the case for the bending energy (see Figure S2b,d in Supporting Information).

Moreover, Figure 4b suggests the process parameter ranges where the selectivity of the incubation times can be dramatically improved by adjusting the reactive hydrogen gas content. At a very low hydrogen content (~2%), the (6,5) and (15,0) nanotubes nucleate within only 1.17 s from each other. When r_H increases to ~15%, this difference dramatically increases to almost 3.0 s. A further increase of the hydrogen content decreases the selectivity, however, much more moderately compared to the initial increase in the 10−20% range. The results in Figure 4b are therefore consistent with the experimentally reported decrease of the SWCNT diameters and narrower chirality distribution after the hydrogen gas pressure was increased in chemically active C_xH_y/H_2 gas mixtures.[20,31]

Therefore, by adjusting the total gas pressure and the percentage of reactive hydrogen in the gas mixture, one can effectively accelerate the SWCNT incubation process and also achieve better nanotube size/chirality selectivity. It is noteworthy that the effectiveness of this control depends on the response time of gas valves and mass flow controllers and the time of establishing the equilibrium in the gas mixture at any particular preset pressure and composition. These times are much longer compared to the almost instantaneous responses of the plasma parameters to the variation of the input power and substrate bias discussed in the previous section.

2.6. Toward Time-Programmed, Size-Selective SWCNT Growth. The results of numerical experiments of the previous sections can be used to develop specific time-programmed processes for size-selective nucleation and growth of single-walled carbon nanotubes using precisely dosed exposure of catalyst nanoparticles to low-temperature, low-pressure thermally nonequilibrium plasmas. This can be achieved by generating plasma discharges of the required parameters for specific time under conditions of continuous substrate heating and precursor gas flow in the same plasma reactor. The substrate heating and the gas flow can also be adjusted in a time-programmed fashion. However, the response time of the external heating is determined by the prevailing heating/cooling rates of the substrate holder which can be quite large. As discussed in the previous subsection, the time to reach equilibrium in the gas flow can also be quite significant. Therefore, given the very short times that separate the nucleation of different nanotubes, the "on" and "off" sequences of the plasma (controlled by the pulsed or limited-time power

dx.doi.org/10.1021/ja210813s | J. Am. Chem. Soc. 2012, 134, 4303−4312

coupling to the gas mixture) and substrate biasing may be the most effective controls to achieve the desired narrow distributions of the nanotube sizes and chiralities.

There are many possibilities to enable the time-programmed, size-selective SWCNT growth and the most important question is when to start the plasma. Our results suggest that igniting the plasma at the very beginning of the process may be more advantageous than after some time into the thermal CVD process. From practical considerations, the process should start by presetting the gas pressure and substrate temperature to the values well below the SWCNT nucleation thresholds in a purely thermal process. For example, the temperature of the substrate holder should be below the minimum temperature for SWCNT nucleation in thermal CVD, which is approximately 590 °C in Figure 2b. The plasma should then be produced to provide the optimum supply of carbon atoms and additional heating to enable fast nucleation of small GMLs not exceeding the desired maximum size. After the incubation time of the largest desired nanotubes elapses, the plasma discharge may be extinguished and the purely thermal CVD continued. After the plasma is switched off, the temperature of the catalyst nanoparticles should be just sufficient to maintain the CVD growth process of the already nucleated nanotubes at the desired rate. Indeed, the amounts of energy required to sustain the growth of the already nucleated nanotubes are notably lower compared to the nucleation stage. The stationary growth temperature should still be lower than the nucleation threshold of thicker nanotubes on the still undersaturated CNPs in a purely thermal CVD process. In this scenario, the plasma acts as a facilitator of nucleation of thin nanotubes which continue to grow to the desired length in a thermal CVD in the same gas mixture.

Another possibility is to adjust the plasma parameters to achieve the similar effect as above instead of completely switching off the plasma discharge right after the nanotubes of the desired maximum thickness nucleate. In this case, the input power and the substrate bias may be reduced to prevent, or at least significantly slow down, the nucleation of thicker nanotubes. In the latter case, the already nucleated thinner nanotubes (which require smaller amounts of carbon atoms per unit length) may reach considerable lengths while the caps of thicker nanotubes just start nucleating and lifting off the CNP surfaces. In this way, the thicker nanotubes can be effectively drowned out in a much taller forest of thinner SWCNTs of the required maximum size.

It is important to stress that the dependences of the nanotube incubation times on the process parameters are nonlinear and these nonlinearities appear to be stronger for thinner nanotubes on smaller catalyst nanoparticles. For example, the nucleation barriers increase very steeply below a certain CNP size.[17] In this way, one can adjust the time-limited plasma exposure to nucleate SWCNTs within the certain diameter range, for example, 0.7−0.9 nm most frequently observed in the plasma-based experiments.[15,17−20,29−31] In this case, the combined amount of the externally supplied and the plasma-produced heat should be insufficient to nucleate the very thin nanotubes below the minimum desired diameter range.

The above examples do not exclude all the possibilities to achieve the desired SWCNT size distributions and selectivity by tailoring the time-programmed plasma exposure. For example, plasma-assisted nucleation of short nanotubes of the desired diameters may be combined with the following pulses of purely etching plasmas by intermittent disruptions of hydrocarbon precursor supply. In this case, any graphene fragments or complete GML nuclei of the thicker nanotubes which have not yet bent or their just-formed caps may be effectively etched away, alongside with the unwanted amorphous carbon on or around the catalyst nanoparticles.

2.7. A Word of Caution. The results of our numerical experiments have suggested that small CNPs produce better results in terms of the nanotube size distribution and selectivity. However, it is critical that the external heating temperature should remain as low as possible, ideally below the lowest nucleation threshold for thermal CVD (which is approximately 590 °C in Figure 2d) as mentioned in the previous subsection. Indeed, under such conditions not only supersaturation of larger nanoparticles (and hence SWCNT nucleation on them) can be substantially decelerated, but also the highly undesirable coagulation of small CNPs into larger agglomerates can be avoided; the latter is a common artifact of many thermal CVD processes, especially at process temperatures exceeding ∼700 °C.[36] If this coagulation nevertheless happens, according to the results in Figure 2d, one can expect an almost simultaneous nucleation of nanotubes with a very broad size distribution. This trend is commonly observed experimentally in thermal CVD.[22,36]

There are further benefits of using plasmas to improve the quality and rates of the nanotube nucleation and growth. The effective CNP surface conditioning can be achieved through the interaction of ions and reactive hydrogen atoms with the surface. In this way, amorphous carbon can be removed very effectively, not only from the catalyst surface, but also from the areas around the catalyst. Other impurities can also be effectively removed through the plasma-surface interactions on the catalyst nanoparticle surface. These interactions significantly reduce the risk of catalyst burying by amorphous carbon and also improve the structural quality of the SWCNT nucleus and the SWCNT walls at later growth stages. The energy of the plasma ions should not be too high, otherwise unnecessary damage could be caused. However, the surface bombardment by moderate-energy ions may also lead to the improvement of the structural quality of the nanotubes, similar to the well-known ion-induced amorphous-to-crystalline phase transitions and crystal densification. This effect still awaits its conclusive confirmation for the SWCNT nucleation and growth in a plasma.

3. SUMMARY AND CONCLUSIONS

The numerical experiments in this study have demonstrated a viable possibility to control the incubation times of single-walled carbon nanotubes by tailoring the nanoscale reactive low-temperature plasma chemistry on the surfaces of metal nanoparticles that catalyze the nanotube nucleation and growth. The multiphase, multiscale computations are based on a combination of several models that intimately interlink the elementary processes of energy and matter exchange in the plasma sheath, on the surface and inside the Au CNPs.

The nanoscale reactive plasma chemistry is controlled by the ion-assisted carbon atom production, effective heat exchange through the ion bombardment and recombination of the plasma radical species, and some other plasma-specific processes. Compared to bulk surfaces, the NRPC is unique because it unfolds on the surfaces and within the catalyst nanoparticles that offer unique conditions for the diffusion and nucleation of carbon atoms to take place. One of the most

unique and, as it turned out, very useful NRPC conditions was provided by the size-dependent Gibbs−Thomson effect, which constructively interplayed with the localized plasma heating and species production effects. This interplay strongly enhanced the bending of stable graphene monolayer nuclei, the key step in the formation of stable SWCNT caps. These unique NRPC elementary processes have resulted in a much faster GML nucleation on small catalyst nanoparticles, at markedly lower external heating temperatures in PECVD compared to purely thermal CVD. The incubation times and the computed trends have been found in a reasonable agreement with the available experimental results on plasma-based SWCNT synthesis.[17,20,29−31]

Moreover, our numerical experiments have established comprehensive links in the three-dimensional parameter space between the incubation times, minimum diameters of SWCNTs that are expected to nucleate on catalyst nanoparticles of a given size, and a range of plasma- and precursor gas-specific parameters such as the plasma density, electron temperature, substrate bias, total gas pressure, and percentage of hydrogen etching gas in the mixture. These links have also revealed several features that are due to the uniqueness of the NRPC effects and can be used to precisely tailor the process parameters to control the nucleation of single-walled carbon nanotubes.

Of particular interest is that the interplay of the plasma and size-dependent Gibbs−Thomson effect introduces the additional size-dependent feature in the process, namely, more clearly size-resolved bending of the stable graphene nuclei. This in turn has resulted in more clearly distinct moments of nucleation of SWCNTs with different diameters (and hence, chiralities). This feature explains several recent experimental observations of better size/chirality selectivity of thin single-walled carbon nanotubes grown at low temperatures in PECVD.[15,17−20,29−31]

On the basis of these results, we have proposed a generic approach toward developing sophisticated time-programmed PECVD based on limited-time or pulse exposure of the catalyst and growing nanotubes to the plasma. This approach is based on the precise knowledge on the incubation times of SWCNTs of the desired thickness/chirality, the relative differences of these times for the nanotubes of different sizes, size- and process-dependent nucleation thresholds, and several other interesting features derived from our numerical experiments.

Our numerical experiments have therefore provided *real-time* information about the most essential *kinetic* characteristic of the SWCNT nucleation, namely, the incubation time and its dependence not only on the catalyst, but also on the parameters of the plasma-based process. For example, it was previously argued[33] that the lower energy of formation for semiconducting tubes as compared to metallic tubes is the main reason for the preferential nucleation of thin semiconducting nanotubes. This study offers alternative, kinetic arguments that complement the existing thermodynamic considerations. Our results suggest that the kinetics behind the SWCNT nucleation is also a major factor in the observed preferential growth, alongside with the proposed thermodynamic stability of the nanotubes.[33] This is one of the most important conclusions of this work. The argument of thermodynamic versus kinetic nucleation/growth has been a long-standing question in the nanotube growth and most of the existing models have focused on the thermodynamic arguments. Furthermore, unlike most of the existing modeling approaches, our approach encompassed the most essential elements of this process *in its entirety*. As such, it can be *used by experimentalists* to develop a variety of CVD-based nanotube synthesis processes. Many of the revealed control features are due to the *nanoscale reactive plasma chemistry* which appears to be a very powerful, yet poorly explored tool to enable time-programmed, size/chirality-selective synthesis of thin single-walled carbon nanotubes at low process temperatures and feedstock gas pressures.

The results and proposed approaches of this study are generic and can be used for a large number of nanoscale synthesis processes and materials systems not merely limited to carbon nanotubes or one-dimensional nanostructures. Future efforts are expected to include later stages of the SWCNT growth, to improve the qualitative agreement with the experimental results, as well as to explain real-time, selective nucleation of graphene layers, nanocages, nanowires, and some other nanostructures. Finally, careful introduction of such *real-time, kinetic-controlled* numerical modeling approaches into experimental practice will eventually make the ultimate dream of chirality-controlled thin single-walled carbon nanotube synthesis at low, device-tolerant process temperatures a laboratory-scale, and eventually, commercial reality.

4. MODELS AND COMPUTATIONAL METHODOLOGY

As mentioned in secction 2.1, our multiscale, multiphase model comprises the plasma sheath, ion/radical transport (Module 1, Figure 1b), species creation/loss, plasma-surface interactions, heat transfer, surface/bulk diffusion (Module 2, Figure 1c), as well as catalyst nanoparticle saturation, graphene monolayer nucleation, and bending/lift-off numerical modules (Module 4, Figure 1d,e). Module 1 includes sets of equations that describe the transport of the selected neutral and charged species in the plasma sheath, their energies and fluxes onto the surfaces of the substrate and catalyst nanoparticles. This module links the parameters of the plasma bulk to the surface conditions and also calculates the electric fields in the vicinity of the CNPs; these electric fields induce polarization effects and affect surface mobility and nucleation of carbon atoms.

Module 2 includes mass and energy balance equations on the surface of Au catalyst nanoparticles which account for contributions from a large number of thermal and plasma-specific chemical reactions, such as, for example (see Figure 1c), thermal dissociation (TD) of main radical species

$$CH_{3(surface)} \rightarrow C_{(surface)} + H_{(surface)} + H_{2(sheath)}$$

ion-induced radical/molecular dissociation (IID)

$$CH^{+}_{3(sheath)} + CH_{3(surface)} \rightarrow C_{(surface)} + H_{(surface)} + H_{2(sheath)} + CH^{+}_{3(sheath)}$$

ion decomposition (ID)

$$CH^{+}_{3(sheath)} \rightarrow C_{(surface)} + H_{(surface)} + H_{2(sheath)}$$

hydrogen atom recombination (HR)

$$H_{(surface)} + H_{(sheath)} \rightarrow H_{2(sheath)} + 4.5\ eV$$

and hydrogen ion neutralization (HIN)

$$H_{(surface)} + H^{+}_{(sheath)} \rightarrow H_{2(sheath)} + 13.2\ eV$$

on the CNP surface of temperature T_S, which is calculated as a function of the substrate holder temperature T_h. Surface (SD) and bulk (BD) diffusion of C species are described using the input from Module 1 and the radical/atom production/loss equations and taking into account the plasma-affected temperature of the CNP, as well as the effects of the polarizability/nonuniform electric field on the diffusion/mobility of carbon atoms. The heat balance equations,

complemented with appropriate boundary conditions, are used to compute the nanoparticle temperature and its difference from the temperature of the substrate holding platform.

Module 3 takes into account the temperature- and size-dependent solubility of carbon atoms in the Au CNP, their extrusion to the CNP surface, and calculates the difference between the chemical potentials within the catalyst nanoparticle and its surface; this difference is the driving force for the GML nucleation on the CNP surface. It is assumed that due to the plasma- and polarization/electric field-related effects the GML starts nucleating at the topmost position of the CNP in contrast to thermal CVD where nucleation with random orientation is expected. This assumption has recently been confirmed by atomistic simulations of SWCNT nucleation in the presence of a vertically oriented electric field.[34] The kinetic equation for the GML nucleation takes into account the size-dependent Gibbs–Thomson effect.[35] This effect reduces the supersaturation within smaller CNPs more significantly compared to larger nanoparticles and leads to the faster extrusion of dissolved carbon atoms to the surface. It is important to emphasize that the Gibbs–Thomson and the plasma-specific effects act synergistically to enhance (and speed up) the extrusion of carbon species to the upper CNP surface. Indeed, more effective carbon production on the plasma-exposed CNP surface and additional heating facilitate the GML nucleation process. Moreover, both the plasma and the GT effects facilitate melting of catalyst nanoparticles, which becomes easier as their curvature increases (this is another manifestation of the GT effect).[21,37]

In this module, the minimum energy and the critical diameter for stable GML formation, as well as the bending energy of the GML sheet, are computed and are intimately related to the surface and the plasma parameters imported from Modules 1 and 2.

The moment $t = t_i$ of the formation of the GML is considered as the incubation time. The incubation time $t_i = t_d + t_p$ is an important kinetic characteristic of the nanotube nucleation process since it includes the times required for carbon atoms to dissolve into the CNP (t_d) and then precipitate (t_p) at the CNP's surface. These times are related to the number of deposited carbon atoms N_C and their fluxes J_V and J_S through the bulk and over the surface of the nanoparticle, as determined by eqs (S-14) and (S-15) in the Supporting Information. Importantly, the times t_d and t_p also depend on the activation energies of several elementary surface processes (e.g., surface diffusion barrier) which are in turn related to the fundamental thermodynamic characteristics of the atomic bonds of the surface. As such, the incubation time incorporates the important features of both thermodynamic and kinetic processes. Please note that our definition of t_i is quite different from the incubation time derived from experiments (the onset of first clearly resolvable PLE signals). The model does not account for the possible changes of the nanotube chirality during the growth process, which may happen, for example, due to defect incorporation.[11]

In this work, Au was chosen as catalyst material rather than more commonly used Fe, Co, and various alloys. One of the main reasons is the strong response of the Au catalyzed-SWCNT nucleation to the presence of hydrogen in the plasma. Indeed, hydrogen addition to the working gas mixture led not only to smaller SWCNT diameters, but also to better chirality selectivity. In contrast, no significant selectivity was observed when Fe nanoparticles were used for the SWCNT growth.[20] Therefore, Au nanoparticles are good alternatives for SWCNT nucleation when more hydrogen containing gases are used in the synthesis. Besides, the solubility of carbon in small Au nanopraticles can be more than 3 times higher compared to the bulk Au,[38] which further substantiates the SWCNT growth observed in many experiments.[20,39,40]

For more detailed description, main assumptions, and limitations of the specific modules within our model please refer to the Supporting Information and our previous publications.[21,32,41]

■ ASSOCIATED CONTENT

Supporting Information

Details of the main equations, assumptions, and limitations of the models used in our numerical experiments, additional results on the dependence of GML bending energy on the CNP radius and substrate holder temperature and on the effect of the total gas pressure and percentage of hydrogen on the GML critical diameter and bending energy, as well as additional comments on the consistency of these computations with the available experimental results. This material is available free of charge via the Internet at http://pubs.acs.org.

■ AUTHOR INFORMATION

Corresponding Author

Kostya.Ostrikov@csiro.au

Author Contributions

†These authors contributed equally.

Notes

The authors declare no competing financial interest.

■ ACKNOWLEDGMENTS

This work was partially supported by the Australian Research Council and CSIRO's OCE Science Leadership Program. H.M. acknowledges supports by the University of Sydney International Scholarship, CSIRO OCE top-up scholarship, and University of Mazandaran PhD program.

■ REFERENCES

(1) Baughman, R. H.; Zakhidov, A. A.; De Heer, W. A. *Science* **2002**, *297*, 787.
(2) Meyyappan, M., Ed.; *Carbon Nanotubes: Science and Applications*; CRC Press: Boca Raton, FL, 2004.
(3) Futaba, D. N.; Hata, K.; Yamada, T.; Hiraoka, T.; Hayamizu, Y.; Kakudate, Y.; Tanaike, O.; Hatori, H.; Yumura, M.; Iijima, S. *Nat. Mater.* **2006**, *5*, 987.
(4) Javey, A.; Guo, J.; Wang, Q.; Lundstrom, M.; Dai, H. *Nature* **2003**, *424*, 654.
(5) Crouse, C. A.; Maruyama, B.; Colorado, R. Jr..; Back, T.; Barron, A. R. *J. Am. Chem. Soc.* **2008**, *130*, 7946.
(6) Ding, F.; Harutyunyan, A.; Yakobson, B. *Proc. Natl. Acad. Sci. U.S.A.* **2009**, *106*, 2506.
(7) Neyts, E. C.; Shibuta, Y.; van Duin, A. C. T.; Bogaerts, A. *ACS Nano* **2010**, *4*, 6665.
(8) Tam, E.; Ostrikov, K. *Appl. Phys. Lett.* **2008**, *93*, 261504.
(9) Page, A. J.; Yamane, H.; Ohta, Y.; Irle, S.; Morokuma, K. *J. Am. Chem. Soc.* **2010**, *132*, 15699.
(10) Shibuta, S. *Carbon* **2011**, *20*, 334.
(11) Neyts, E. C.; van Duin, A. C. T.; Bogaerts, A. *J. Am. Chem. Soc.* **2011**, *133*, 17225.
(12) Kanzow, H.; Lenski, C.; Ding, A. *Phys. Rev. B: Condens. Matter Mater. Phys.* **2001**, *63*, 125402.
(13) Meyyappan, M. *J. Phys. D: Appl. Phys.* **2009**, *42*, 213001.
(14) Chiang, W.-H.; Sankaran, R. M. *Nat. Mater.* **2009**, *8*, 882.
(15) Hatakeyama, R.; Kaneko, T.; Kato, T.; Li, Y. F. *J. Phys. D.: Appl. Phys.* **2011**, *44*, 174004.
(16) Keidar, M. *J. Phys. D: Appl. Phys.* **2007**, *40*, 2388.
(17) Kato, T.; Hatakeyama, R. *ACS Nano* **2010**, *4*, 7395.
(18) Volotskova, O.; Fagan, J. A.; Huh, J. Y.; Phelan, F. R. Jr.; Shashurin, A.; Keidar, M. *ACS Nano* **2010**, *4*, 5187.
(19) Sankaran, R. M. *J. Phys. D.: Appl. Phys.* **2011**, *44*, 174005.
(20) Ghorannevis, Z.; Kato, T.; Kaneko, T.; Hatakeyama, R. *J. Am. Chem. Soc.* **2010**, *132*, 9570.
(21) Ostrikov, K.; Mehdipour, H. *ACS Nano* **2011**, *5*, 8372.

(22) Han, Z. J.; Yick, S.; Levchenko, I.; Tam, E.; Yajadda, M. M. A.; Kumar, S.; Martin, P. J.; Furman, S.; Ostrikov, K. *Nanoscale* **2011**, *3*, 3214.
(23) Ostrikov, K. *Rev. Mod. Phys.* **2005**, *77*, 489.
(24) Cvelbar, U.; Chen, Z. Q.; Sunkara, M. K.; Mozetic, M. *Small* **2008**, *4*, 1610.
(25) Xu, S.; Xiao, S. Q. *J. Phys. D: Appl. Phys.* **2011**, *44*, 174033.
(26) Shieh, J.; Hou, F. J.; Chen, Y. C.; Chen, H. M.; Yang, S. P.; Cheng, C. C.; Chen, H. L. *Adv. Mater.* **2010**, *22*, 597.
(27) Melechko, A. V.; Merkulov, V. I.; Lowndes, D. H.; Guillorn, M. A.; Simpson, M. L. *Chem. Phys. Lett.* **2002**, *356*, 527.
(28) Mariotti, D.; Svrcek, V.; Kim, D.-G. *Appl. Phys. Lett.* **2007**, *91*, 183111.
(29) Li, Y.; Mann, D.; Rolandi, M.; Kim, W.; Ural, A.; Hung, S; Javey, A.; Cao, J.; Wang, D.; Enilmez, E.; Wang, Q.; Gibbons, J. F.; Nishi, Y.; Dai, H. *Nano Lett.* **2004**, *4*, 317.
(30) Qu, L.; Du, F.; Dai, L. *Nano Lett.* **2008**, *8*, 2682.
(31) Kato, T.; Hatakeyama, R. *J. Nanotechnol.* **2010**, *11*, 490529.
(32) Ostrikov, K.; Mehdipour, H. *J. Mater. Chem.* **2011**, *21*, 8183.
(33) Li, Y.; Peng, S.; Mann, D.; Cao, J.; Tu, R.; Cho, K. J.; Dai, H. *J. Phys. Chem. B.* **2005**, *109*, 6968.
(34) Neyts, E. C.; van Duin, A. C. T.; Bogaerts, A. *J. Am. Chem. Soc.* **2012**, *134*, 1256.
(35) Dubrovskii, V. G.; Cirlin, G. E.; Soshnikov, I. P.; Tonkikh, A. A.; Sibirev, N. V.; Samsonenko, Yu. B.; Ustinov, V. M. *Phys. Rev. B.: Condens. Matter Mater. Phys.* **2005**, *71*, 205325.
(36) Naumov, A.; Kunestov, O. A.; Harutyunyan, A. R.; Green, A. A.; Hersam, M. C.; Resasco, D. E.; Nikolaev, P. N.; Weisman, R. B. *Nano Lett.* **2009**, *9*, 3203.
(37) Shiozawa, H.; Kramberger, C.; Pfeiffer, R.; Kuzmany, H.; Pichler, T.; Liu, Z.; Suenaga, K.; Kataura, H.; Silva, S. R. P. *Adv. Mater.* **2010**, *22*, 3685.
(38) Sutter, E. A.; Sutter, P. W. *J. Mater. Sci.* **2011**, *46*, 7090.
(39) Bhaviripudi, S.; Mile, E.; Steiner, S. A. III; Zare, A. T.; Dresselhaus, M. S.; Belcher, A. M.; Kong, J. *J. Am. Chem. Soc.* **2007**, *129*, 1516.
(40) Ghorannevis, Z.; Kato, T.; Kaneko, T.; Hatakeyama, R. *Jpn. J. Appl. Phys.* **2010**, *49*, 02BA01.
(41) Mehdipour, H.; Ostrikov, K.; Rider, A. E. *Nanotechnology* **2010**, *21*, 455605.